COR1 Breadboard #2 Measurements at the NCAR Vacuum Tunnel Facility May–June 2001

William Thompson
June 18, 2001

1 Introduction

This is a report discussing the measurements of the second version of the COR1 breadboard, made at the NCAR Vacuum Tunnel Facility in Boulder, Colorado, during May–June, 2001. Measurements of the first version were taken during the month of March, 2001, and are discussed in a previous report. This breadboard was then modified, and the same measurements were repeated on this modified version. In this report, we discuss this second series of measurements. Details of the measurement process not covered here can be found in the first document.

In the first version of the breadboard, all the optical elements were installed on Newport LP-2 holders. In the second version being reported on here, the objective and field lens assemblies were both mounted in a flight-like cylindrical structure, with baffling between the two lenses. This cylinder section is shown in Figure 1. Behind the field lens assembly (to the left in Figure 1), the focusing lens assembly with the Lyot stop is mounted in a Newport LP-2 holder, as in the first measurement run. Another change that was made was to have two focusing lens assemblies, one which also included a Lyot spot, and another which did not as in the first test. During the test run being discussed here, measurements were first made on the assembly without the Lyot spot. This was then swapped out for the assembly with the Lyot spot.

2 Objective lens cleanliness

Before the breadboard was wrapped for shipment to Colorado, the objective lens was examined by shining a very powerful "Sun Gun" through it via the field lens. An area of some kind of contamination was seen on the front surface of the objective lens approximately to the lower left of center. This feature had not been seen when the lens had first come back from cleaning. The rest of the lens looked fairly clean, except for a small amount of stray dust particles. Overall, the objective lens looked much cleaner than the lenses did in the first test.

This examination process was repeated when the breadboard was unwrapped in Colorado, with no apparent changes. At the end of the measurement run, we examined it once again. In this last examination, it appeared that there might have been a few more random dust particles spread out over the surface of the lens, but it was otherwise unchanged. At the time of this writing, the breadboard has not yet been unwrapped and examined after having been shipped back to Goddard.

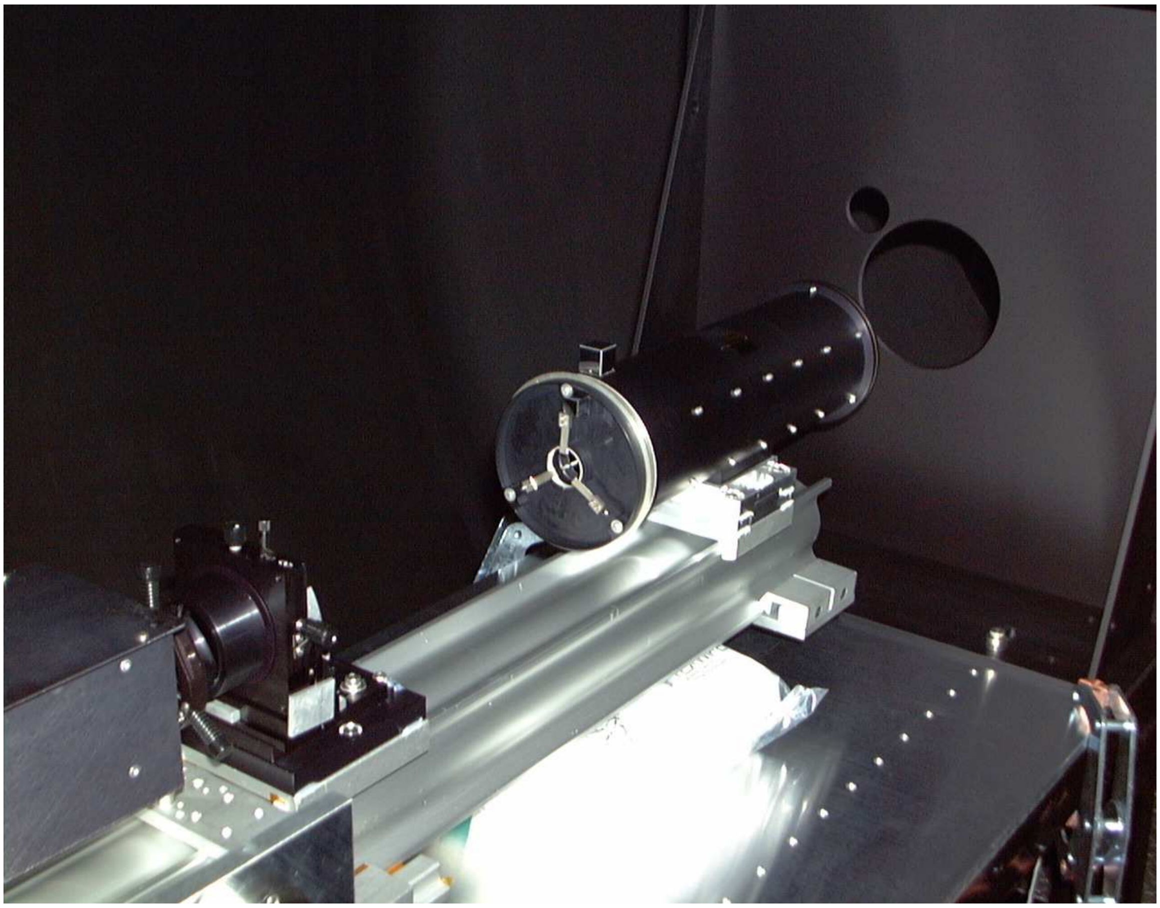

Figure 1: Photograph of the front cylindrical section of the second breadboard. The near side of the cylinder contains the field lens, with the embedded occulter on the interior side. The objective lens is mounted on the far side. Also visible on the left side of the photograph is the focusing lens assembly in the Newport LP-2 mount, the bandpass filter, and the baffling which extends back to the detector.

3 Instrument calibration

The same process as before was used to cross-calibrate the breadboard detector and monitoring photodiode. After all the measurements had been made with the optics installed, the optics were removed, allowing the beam to fall directly onto the detector. With this setup, we measured a count rate of $I_0 = 1647 \pm 24$ DN/sec/nA. This can be compared to 1611 ± 70 DN/sec/nA from March, which is the same within the error bars.

In order to use this number to derive the equivalent intensity I of a focused source image, one must include part of the optical prescription of the instrument. The result can be expressed as

$$I = I_0 \times \left(\frac{R_a}{R_i}\right)^2 \times F_g \times F_t \times \left(\frac{D_d}{D_p}\right)^2$$

where the parameters are as follows: $R_a = 18$ mm is the radius of the front aperture, and $R_i = 2.626$ mm is the measured radius of the source image on the detector, so the ratio $(R_a/R_i) = 47$ is the concentration factor of the optical system. F_g represents the geometrical losses from the Lyot stop and spot, where $F_g = 0.931$ without the Lyot spot, and $F_g = 0.875$ with the Lyot spot. $F_t = 0.738$ is the combined transmission of all the lens elements, where the losses are from reflections at each lens surface. Finally, $(D_d/D_p)^2 = 1.09$ gives a correction due to the different distances of the detector and photodiode from the source, as explained in the original report.

Although, the detector itself did not change, the aperture radius R_a and the geometric factor F_g are both different in the new breadboard from their values for the first breadboard. Thus, the extrapolated full-Sun intensities are $I = 5.46 \times 10^4$ and 5.81×10^4 DN/sec/nA for with and without the Lyot spot respectively.

3.1 Additional calibration considerations

In the first breadboard test, some questions were raised about the absolute brightness of the source, and the transmission of the waveband filter. For the second series of measurements, a separate calibrated photometer was taken along (along with an extra bandpass filter). Simultaneous measurements of the beam intensity with the photodiode and the photometer yielded roughly the same values, with the diode readings being consistently 51 ± 3 percent higher than those from the photometer.

Measurements were also taken with the photometer with and without the bandpass filter, showing that the bandpass filter cuts down the light intensity by a factor of 30.

We also took the photometer out to the heliostat platform, and measured the intensity of the sunlight directly, through the bandpass filter. Although these measurements were taken at a different time from the measurements in the tunnel, and thus subject to some uncertainty in the steadiness of the illumination, one can still infer that the beam in the tunnel is on the order of $\sim 10^{-5}$ of the solar brightness. This is consistent with the brightness inferred from the first round of measurements.

It should be pointed out that the instrument calibration does not depend on the absolute intensity calibration of the beam, since all measurements are ratioed to the photodiode readings. The only requirement is that photodiode and CCD detector both be stable. All indications are that

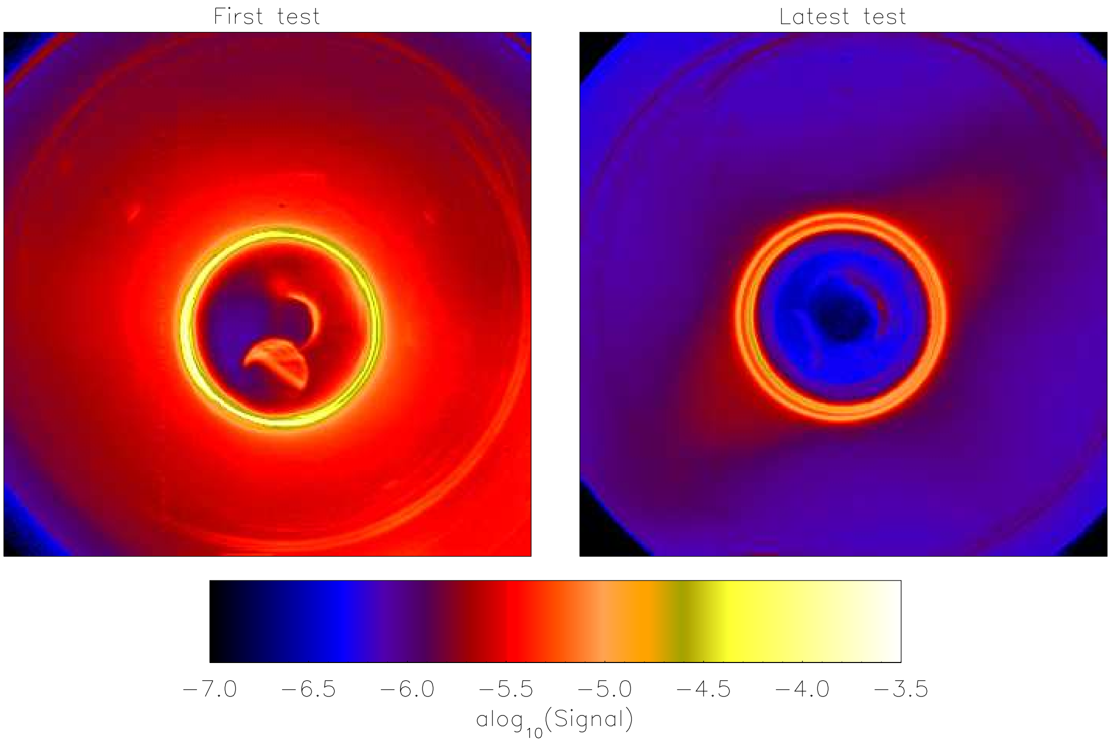

Figure 2: Comparison of the scattering seen in the first breadboard on the left, and the second breadboard on the right. Both measurements were made without a Lyot spot.

this requirement has been met. The absolute calibration of the bandpass filter is also irrelevant, since identical filters were used in front of both the photodiode and detector at all times.

4 Scattering measurements

The first set of measurements were taken with the focusing lens assembly which did not include a Lyot spot. This was later replaced with an identical lens assembly with a Lyot spot installed. Figure 2 shows the comparison between the data taken on the first breadboard in March, and the latest data. There are a number of differences. Both the general level of scattering and the bright ring around the occulter are lower for the new breadboard design. There are ghost images visible in both images within the occulter shadow, but the ghosts are also fainter (presumably because the ring around the occulter is fainter).

Figure 3 shows the comparison between the data taken with and without the Lyot spot in place. It's clear that the inclusion of the Lyot spot makes a big difference in the overall scattering level. Horizontal traces across these images through the approximate center of the occulter shadow are shown in Figure 4. These plots show that a tremendous improvement has been achieved in the scattering profile. The profile with the Lyot spot included, as shown in Figure 4, approaches the

One feature that's evident in Figure 3, particularly in the data taken with the Lyot spot, is that

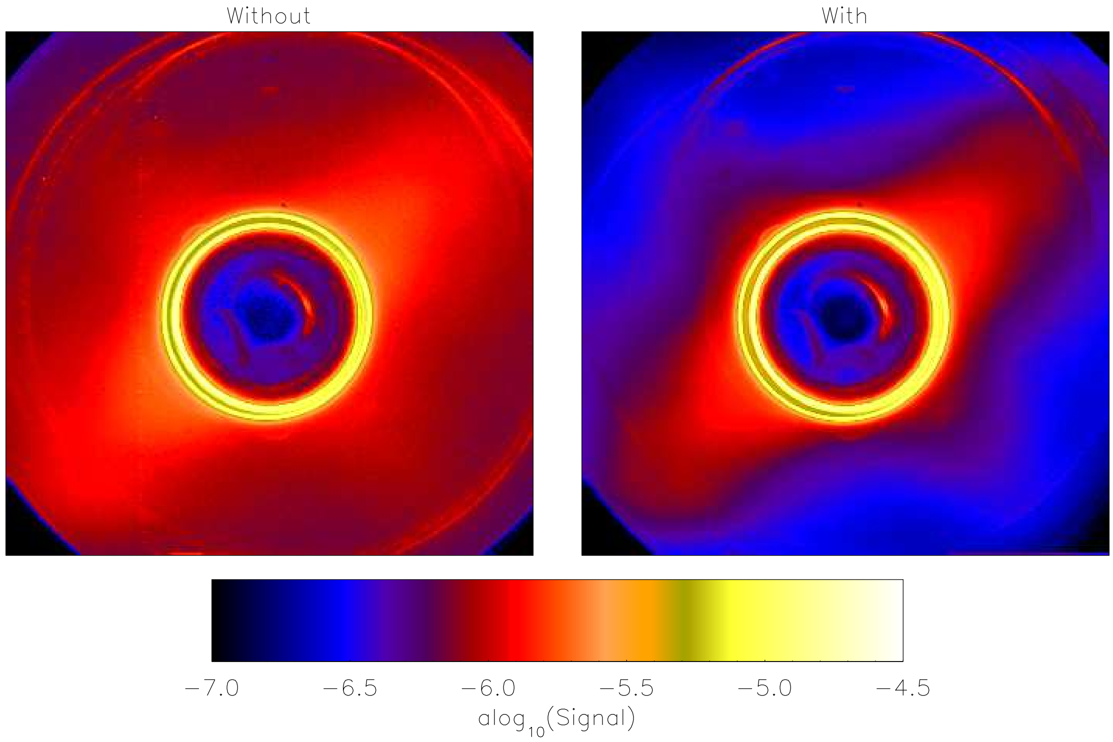

Figure 3: Comparison of the scattering levels of the new breadboard design, taken both without a Lyot spot (left), and with a Lyot spot (right).

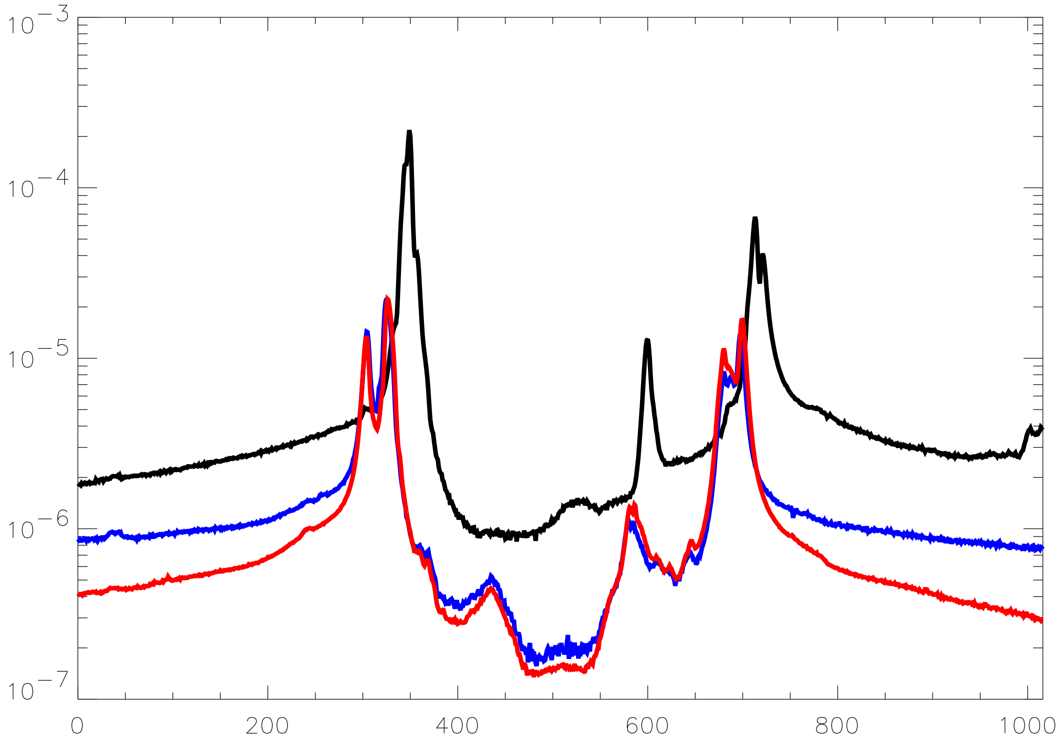

Figure 4: Horizontal traces through the approximate centers of the occulter shadows for breadboard #1 (black), breadboard #2 without the Lyot spot (blue), and with the Lyot spot (red). The full range of this plot is approximately $8R_{\odot}$

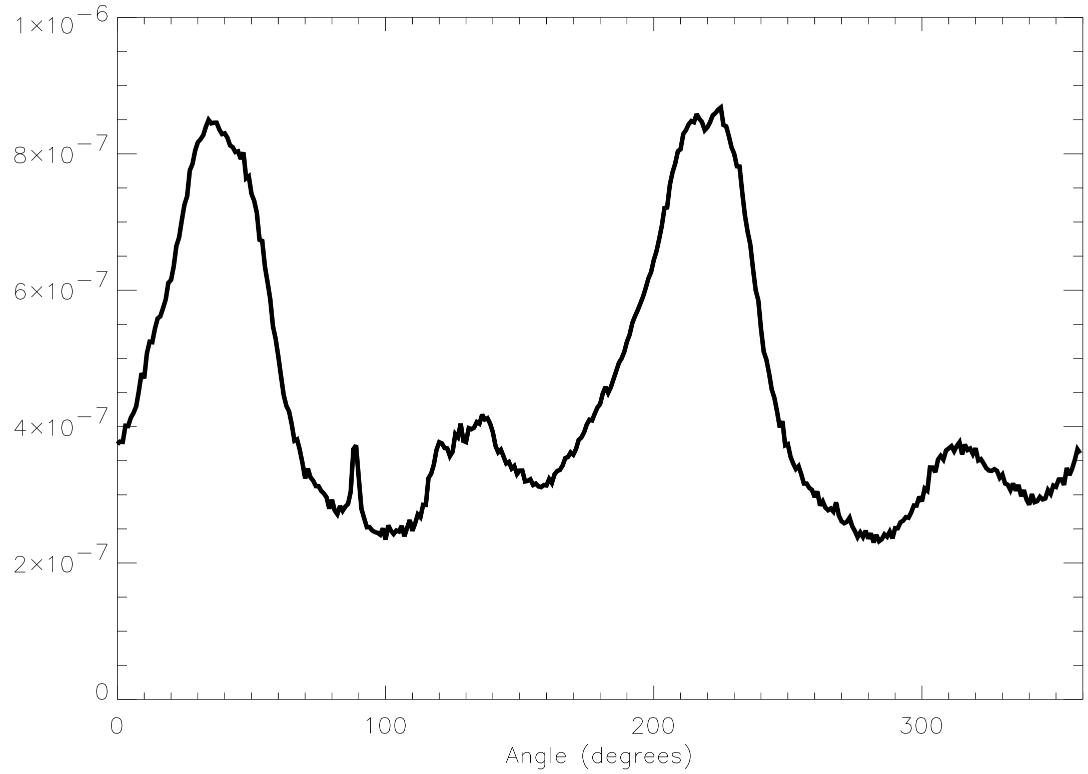

Figure 5: Azimuthal trace at a radius of 3.5 $R_{\odot}$ for the scattering profile with a Lyot spot.

there are areas of enhanced scattering at certain azimuthal angles. Two prominent regions occur at about 2 and 8 o'clock, but there are also less prominent regions at about 5 and 11 o'clock. This is well demonstrated in Figure 5, which shows a circular trace through the data at a radius of 3.5 $R_{\odot}$. One of the tests sequences that was performed was to scan the orientation of the breadboard so that the source image would move from one side of the occulter to the other, just barely avoiding the edge of the occulter at either end. Scans were done both horizontally and vertically. Movies were made from these test sequences, and show quite clearly that these spoke-like features move so as to maintain a constant relationship to the source. The effect is as if these features were part of the source, like coronal streamers surrounding the solar disk. The most likely explanation is that these scattering features are being produced within the objective lens. Another possible, although unlikely, explanation is that they represent some kind of scattering within the vacuum tunnel.

4.1 Bright rings and occulter shadow

It's quite evident from Figure 3 that there are actually two bright rings near the edge of the occulter. Careful examination of the data from the first test also shows evidence of two rings, but unevenly illuminated, and not so widely separated.

To determine how the two rings are related to the occulter, we measured the radius of each ring, and compared them to the radius of the occulter shadow from an image where we diffusely illuminated the objective with a flashlight. The radii of the two bright rings were 177.7 and

198.4 pixels respectively, while the radius of the occulter shadow was about halfway in between at 186.8 pixels. Thus, one of the rings is just outside the occulter shadow, while the other is just inside. This behavior also appears to hold for the data taken on the first version of the breadboard in March, as far as can be determined.

The pixel location of the center of the two rings does not quite match up with the center of the occulter shadow. When the two images are compared together, the occulter shadow appears to coincide with the inner ring on the left side of the image, and with the outer ring on the right side. However, the occulter shadow image was taken before the rail was completely installed into the vacuum chamber, and a small shift may have occured during the completion of the installation process, such as the attachment of the cooling lines.

If the occulter shadow radius of 186.8 pixels represents 1.5 $R_\odot$, then we can infer that the detector plate scale is about 0.008 $R_\odot$/pixel.

4.2 Ghosts and arcs

Most of the observations were made with a 100 second exposure. We also made a few observations with exposure times of 30 seconds and 300 seconds, to check the operation of the shutter, and even one with an exposure time of 1000 seconds. The result of the 1000 second exposure is shown in Figure 6. (Although the bright rings around the occulter edge are saturated with this exposure time, a larger area appears to be saturated in Figure 6 than actual because the image has been stretched to bring out the fainter features.) A number of ghosts and arcs are visible. Some of the arcs near the edges of the image are caused by the shutter housing, but the large bright arc along the top cannot be attributed to the shutter.

4.3 Filter position

The commercial bandpass filter that was used has a very shiny surface. In order to test how this filter might be related to the various ghost images and arcs, tests were done with the filter in three different positions. The standard position for the filter was immediately behind the focusing lens, as shown in Figure 1. Also tested was in front of the focusing lens, and in front of the camera. The results are shown in Figure 7. These data were taken in air, so the camera could not be cooled. Thus, only the brighter arcs are visible above the increased noise floor. Those features which are visible do not show any changes between filter positions, although there are changes in the overall scattering profile. (Because the camera is warm, there is an additional feature at the very top which appears in these images as a dark wedge with a bright rim, and is caused by bleeding within the CCD.)

5 Derived profiles

From Figure 5, one can see that the worst scattering behavior occurs at an azimuthal angle of about 40°, there is another peak perpendicular to this at about 130°, and the best behavior occurs at about 105°. Figure 8 shows radial traces at these three angles. If we ignore the bright ring at the edge of the occulter, the overall scattering pattern along these three directions can be modeled

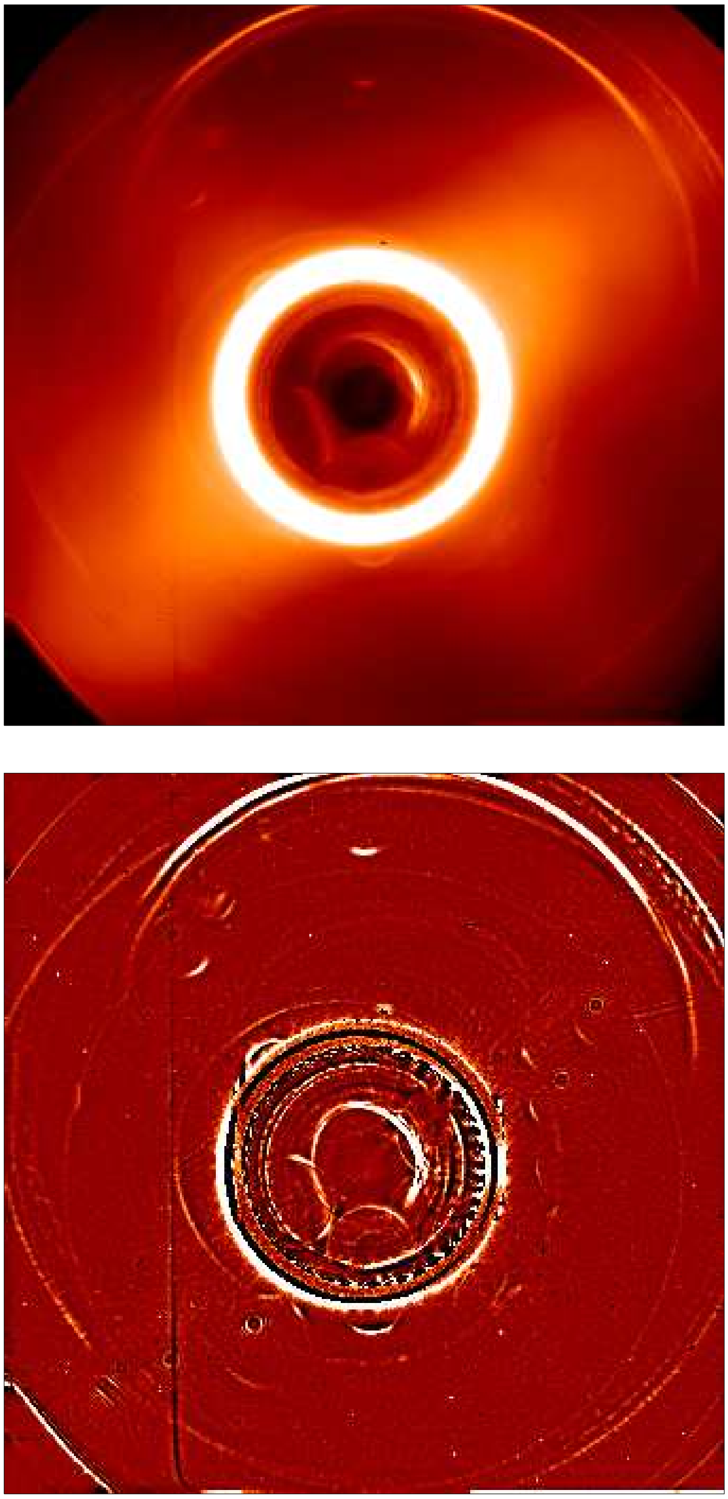

Figure 6: Upper: an image taken with 1000 second exposure, stretched to show the faintest features. Lower: the same image passed through a high bandpass filter. The vertical feature on the left is a camera defect.

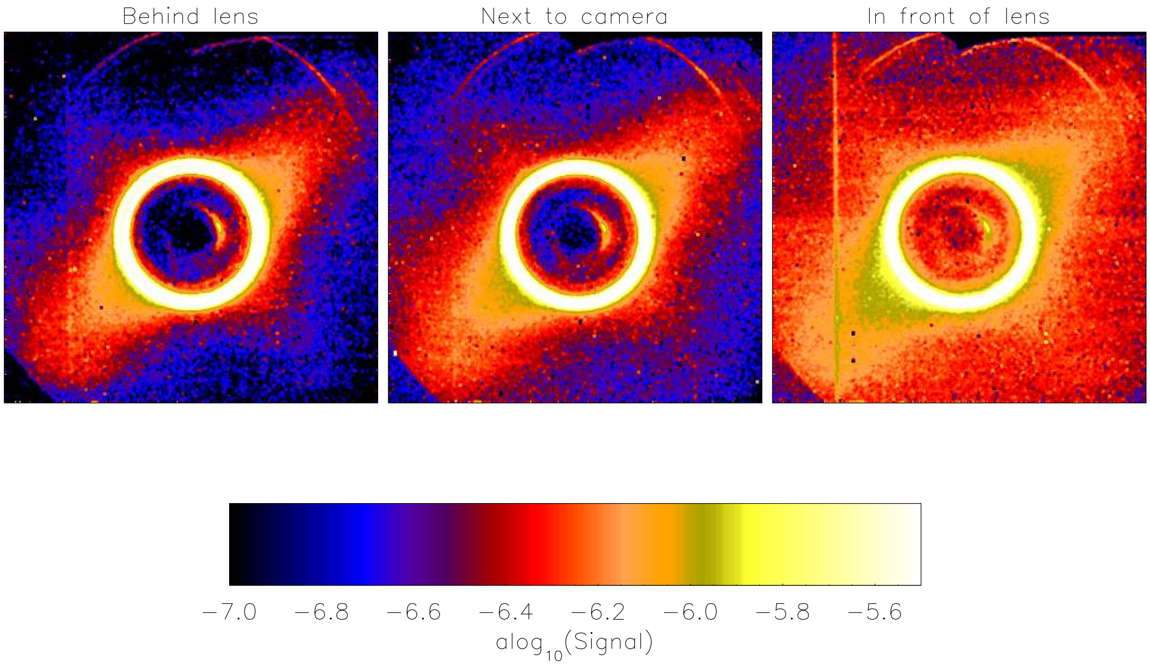

Figure 7: Images taken with the bandpass filter in various positions along the rail.

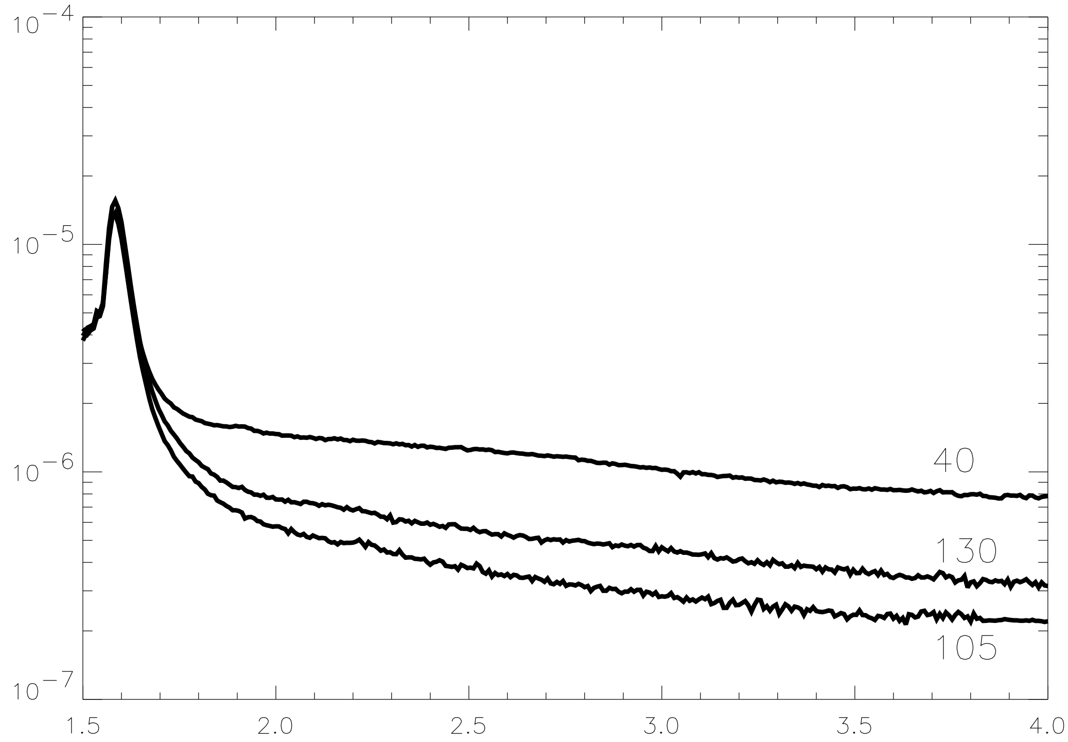

Figure 8: Radial traces from the center of the occulter outwards, at azimuthal angles of 40° and 130°, representing the cross pattern evident in Figure 3, and at 105° where the lowest level of scattering is seen.

as

$$\begin{aligned}
\log_{10} y(40^\circ) &= -5.508 - 0.159x \\
\log_{10} y(130^\circ) &= -5.359 - 0.473x + 0.0473x^2 \\
\log_{10} y(105^\circ) &= -5.050 - 0.794x + 0.0984x^2
\end{aligned}$$

where $x = R/R_\odot$ is the radial distance in solar radii. These equations are valid from approximately $x = 1.8$ out to $x = 4$.

Acknowledgments

The author would like to thank the National Center for Atmospheric Research for the use of the Vacuum Tunnel Facility, and Greg Card for his help during the observations. He would also like to thank John Stewart for his help in making the measurements. Thanks also go to Eric Mentzell for providing correction factors for the Lyot stop, Lyot spot, and reflections from the lens surfaces.